The Effects of Surface Irregularities on the Elastohydrodynamic Lubrication of Sliding Line Contacts. Part I—Single Irregularities

P. R. Goglia[1]

T. F. Conry

C. Cusano

University of Illinois
at Urbana-Champaign,
Urbana, Ill. 61801

A full line contact solution, under isothermal conditions, is obtained in which the effects of single stationary surface irregularities on the EHD lubrication process are studied under pure sliding conditions. The irregularities studied are furrows, furrows with built-up edges, and asperities. The effects of these irregularities on film thickness, pressure, and subsurface octahedral shear stress are presented. The pressure and film thickness resulting from such surface irregularities are significantly changed from their smooth surface values. These changes alter the state of stress in the subsurface region by increasing the maximum value of octahedral shear stress and bringing the location of this maximum stress closer to the surface. The film thickness in the contact is significantly changed from the smooth surface value only when the irregularities are located in the inlet region while the maximum value of the octahedral shear stress increases to the greatest extent when the irregularities are located in the outlet half of the contact.

Introduction

The topography of the surfaces in concentrated contact influences the lubrication process and the associated stress field in the solids, which can significantly contribute to both surface-initiated fatigue failures and scuffing failures of mechanical elements. Surface-initiated fatigue failures can take place as the result of asperity interactions that cause plastic deformation and subsequent micropitting and microcracking of the surfaces. Such failures can also take place as the result of manufacturing processes or service related surface defects. Surface topography is also intimately connected to the events initiating scuffing. The localized surface damage is caused by the solid-phase welding of interacting asperities and the consequent tearing of these welds due to the relative motion of the surfaces. The dominating importance of both surface-initiated fatigue failures and scuffing failures in concentrated contacts has served to increase interest in the study of the effects of surface roughness and surface defects on the lubrication mechanics as it relates to these failures.

One approach that has been taken in studying surface roughness effects is to use models that provide information on the lubrication process only in an average sense. Stochastic roughness models have been used in hydrodynamic lubrication by Tzeng and Saibel [1] and Christensen [2, 3], while Patir and Cheng [4, 5] have proposed a three-dimensional surface model for calculating average flow and average pressure. The line contact EHD lubrication problem with random surface roughness has been solved by Chow and Cheng [6].

With the stochastic approach discussed above, information about the influence of individual surface irregularities cannot be extracted. Thus, important quantities such as peak pressures, maximum values of stress, and minimum film thicknesses caused by these irregularities are not known. This limitation of the stochastic approach can be avoided by studying the effects of a single irregularity on the pressure, subsurface stress, and film thickness profile in EHD lubrication. Such studies have been analytically conducted by Fowles [7], and Cheng and co-workers [8-11].

Experimental studies of rough surfaces under EHD lubrication conditions are very difficult to perform. The rapid changes in surface profile due to random surface irregularities can cause problems in determining the true film profile. Recent experimental studies have concentrated on single and multiple irregularities produced on smooth surfaces. Among

[1] Presently at Hewlett-Packard Company, Disc Memory Division, Boise, ID 83707.

Contributed by the Lubrication Division of THE AMERICAN SOCIETY OF MECHANICAL ENGINEERS and presented at the ASME/ASLE Joint Lubrication Conference, Hartford, Conn., October 18-20, 1983. Manuscript received by the Lubrication Division, November 5, 1982. Paper No. 83-Lub-20.

these studies have been those of Jackson and Cameron [12], Kaneta and Cameron [13], Wedeven [14], Wedeven and Cusano [15], and Cusano and Wedeven [16, 17]. With the exception of [14], where the irregularity was previously formed by debris, all other experimental studies mentioned above were conducted by using artificially produced surface irregularities.

The purpose of this study is to present data on the effects of geometrically simple surface irregularities on the film thickness, the pressure distribution, and the subsurface shear stress field in sliding EHD line contact lubrication under isothermal conditions. The data presented in Part I of this study are an extension of the data presented by Cheng and Bali [11]. They used a Grubin-type solution to study single stationary irregularities in line contact under pure sliding conditions. A full line contact solution is presented in this paper. As in [11] only the pure sliding case with stationary irregularities is considered. Based on the results presented in Refs. [13, 17], these kinematic conditions lead to results that represent an upper bound on film thickness changes for a given irregularity. Such an upper bound implies an upper bound on the changes in pressure and subsurface shear stresses.

Governing Equations

A brief description of the governing equations and their solution will be given. These equations and the technique used for their solution are thoroughly discussed in [18].

The line contact EHD lubrication problem (two elastic rollers) under steady state operating conditions is considered. To obtain steady state conditions, the irregularities are located on the stationary surface (top surface in this study). The x-axis is taken along the moving surface (bottom surface in this study) and the z-axis is taken normal to and directed outward from this surface. The origin of the coordinate system is located at the center of the Hertzian contact.

For the problem under consideration, the Reynolds equation is given by

$$\frac{d}{dx}\left(\frac{\rho h^3}{\eta}\frac{dp}{dx}\right) = 12u\frac{d}{dx}(\rho h) \tag{1}$$

The description of the film profile between two elastic rollers in EHD contact depends on the rigid body separation of the two surfaces and the surface displacements caused by interfacial hydrodynamic pressures. For smooth cylinders, this film profile may be expressed as:

$$h = h_0 + (x^2/2R_1) + (x^2/2R_2) + t_1(x) + t_2(x) \tag{2}$$

The expressions for the displacements $t_1(x)$ and $t_2(x)$, caused by a line pressure distribution along an elastic half-space are given by Timoshenko and Goodier [19]. With the geometry of a surface irregularity described by a function $d(x)$, the film profile between two elastic rollers is given by [18]:

$$h = h_0 + (x^2/2R) - (2/\pi E')\int_{s_1}^{s_2} p(s)\ln((x-s)/s)^2 ds + d(x) \tag{3}$$

The surface irregularity $d(x)$ is described by periodic functions and can be represented by the generalized geometry shown in Fig. 1. In terms of the $x'-d$ axes given in this figure, $d(x')$ is defined as

Nomenclature

a_0,a_1,a_2,a_3 = pressure-viscosity model parameters in the slope transition region
A,B = density model parameters
$\bar{A},\bar{B}$ = AE', BE'
b = $4Rp_0/E'$, Hertzian halfwidth
C = l_2/b, l_3/b, dimensionless furrow and asperity halfwidth
d = defect description as a function of x
d_1,d_2,d_3 = asperity and furrow height parameters
E_1,E_2 = moduli of elasticity of solids one and two
E' = $1/E' = \frac{1}{2}\left(\frac{1-\nu_1^2}{E_1}+\frac{1-\nu_2^2}{E_2}\right)$
$\bar{G}_1,\bar{G}_2$ = $\alpha_1 E', \alpha_2 E'$, primary and secondary material parameters
h,h_0,h_m = film thickness, central film thickness (at $x=0$), minimum film thickness
h_{osm},h_{msm} = central and minimum film thicknesses for smooth surface reference cases
l_1,l_2,l_3,l_4 = asperity and furrow width parameters
p,p_0 = pressure, Hertzian peak pressure
p_a,p_b = transition pressure points for pressure-viscosity model
p_{Hz} = dry Hertzian pressure distribution
p_1 = pressure-viscosity slope break pressure
$\bar{P}_1$ = p_1/E'
R = $R_1R_2/(R_1+R_2)$, equivalent radius
R_1,R_2 = radii of cylinders one and two
s,s_1,s_2 = dummy variable and limit of integration in the x-direction
t_1,t_2 = displacement of the surface of solid one and two
u = one-half the velocity of moving surface
$\bar{U}$ = $\eta_0 u/E'R$, dimensionless velocity parameter
w = load per unit length on EHD contact
$\bar{W}$ = $w/E'R$, dimensionless load parameter
x,y,z = coordinates
x^* = furrow or asperity center location
x' = $x-x^*$, variable used for describing the geometry of the asperity, furrow and furrow with a built-up edge
α_1,α_2 = pressure-viscosity coefficients of two-slope exponential model
Δ = d_2/h_{osm}
η = viscosity
η_0 = viscosity at ambient pressure
ν_1,ν_2 = Poisson's ratios of solids one and two
ρ = fluid density
ρ_0 = fluid density at ambient pressure
$\bar{\rho}$ = ρ/ρ_0
$\sigma_1,\sigma_2,\sigma_3$ = principal stresses in solid
σ_{oct} = τ_{oct}/p_0
σ_{octsm} = τ_{octsm}/p_0
τ_{oct} = octahedral shear stress
τ_{octsm} = octahedral shear stress for the smooth surface reference

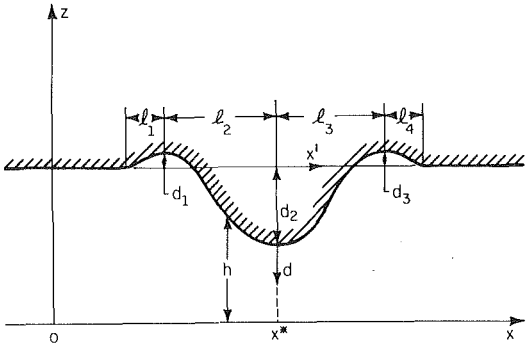

Fig. 1 Generalized geometry of a single surface irregularity

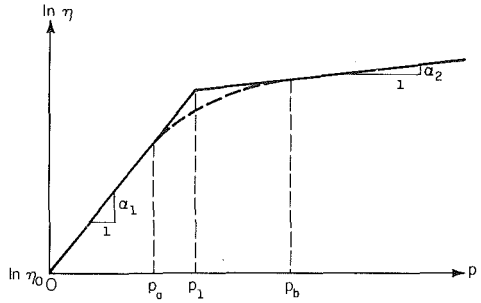

Fig. 2 Two-slope pressure-viscosity model of Allen, Townsend, and Zaretsky [20]

$$d(x') = \begin{cases} 0 & x' \le -(l_1 + l_2) \\ \dfrac{d_1}{2}\left[1 - \cos\left(\dfrac{\pi(x' + l_1 + l_2)}{l_1}\right)\right] & -(l_1 + l_2) < x' < -l_2 \\ d_1 - \dfrac{d_1 + d_2}{2}\left[1 - \cos\left(\dfrac{\pi(x' + l_2)}{l_2}\right)\right] & -l_2 \le x' < 0 \\ -d_2 + \dfrac{d_3 + d_2}{2}\left[1 - \cos\left(\dfrac{\pi x'}{l_3}\right)\right] & 0 \le x' < l_3 \\ \dfrac{d_3}{2}\left[1 + \cos\left(\dfrac{\pi(x' - l_3)}{l_4}\right)\right] & l_3 \le x' < (l_3 + l_4) \\ 0 & x' \ge (l_3 + l_4) \end{cases} \quad (4)$$

Note that the origin of the $x' - d$ axes is located at x^* with the x' axis along a line which coincides with the smooth geometry of the upper surface. The position of x^*, on the x-axis, coincides with the summit of an asperity or the deepest part of a furrow. In this paper the following irregularities are considered: a simple symmetric furrow without a built-up edge, a symmetric furrow with a built-up edge on the outlet side (right side), a symmetric furrow with a built-up edge on the inlet side (left side) and a simple symmetric asperity. Using the symbols given in Fig. 1, these irregularities are described as follows:

1. Simple symmetric flow without a built-up edge has $d_1 = d_3 = l_1 = l_4 = 0$, $l_2 = l_3 > 0$ and $d_2 < 0$.
2. A symmetric furrow with a built-up edge only on the outlet side has $d_1 = l_1 = 0$, $l_2 = l_3 > 0$, $l_4 > 0$, $d_3 > 0$ and $d_2 < 0$.
3. A symmetric furrow with a built-up edge only on the inlet side has $d_3 = l_4 = 0$, $l_2 = l_3 > 0$, $l_1 > 0$, $d_1 > 0$ and $d_2 < 0$.
4. A simple symmetric asperity is the same as a simple furrow except $d_2 > 0$.

Since isothermal conditions are considered in this paper, the viscosity, η, in equation (1) is a function of pressure alone. The pressure viscosity model is a modified version of the two slope exponential model proposed by Allen, Townsend and Zaretsky [20]. The model proposed in [20] is stated mathematically as:

$$\eta = \begin{cases} \eta_0 e^{\alpha_1 p} & p \le p_1 \\ \eta_0 e^{\alpha_1 p_1 + \alpha_2 (p - p_1)} & p > p_1 \end{cases} \quad (5)$$

Equation (5) is represented by the solid shown in Fig. 2.

The behavior of oils under pressure does not suddenly change at $p = p_1$. There must be a smooth transition between the two regions where the differing exponents apply. This concept is illustrated by the dashed line in Fig. 2. The transition may be accomplished by fitting a cubic polynomial to the exponent between points p_a and p_b on the two slopes of the pressure-viscosity model. The general form of this modified pressure-viscosity model then becomes:

$$\eta = \begin{cases} \eta_0 e^{\alpha_1 p} & p \le p_a \\ \eta_0 e^{(a_0 + a_1 p + a_2 p^2 + a_3 p^3)} & p_a < p < p_b \\ \eta_0 e^{\alpha_1 p_1 + a_2 (p - p_1)} & p \ge p_b \end{cases} \quad (6)$$

The coefficients a_0 through a_3 are found by requiring continuity of $\ln(\eta)$ and $\partial(\ln \eta)/\partial p$ at p_a and p_b. For the results presented in this paper p_a and p_b are arbitrarily fixed at $0.75\, p_1$ and $1.4\, p_1$, respectively.

The density, ρ, in equation (1) is also a function of pressure. A model which closely matches experimental data was proposed by Dowson and Higginson [21]. This model is expressed mathematically by

$$\bar{\rho} = \rho/\rho_0 = 1 + [Ap/(1 + Bp)] \quad (7)$$

To obtain a solution to the line contact problem, equation (1) is first discretized using standard second order finite difference forms for variable grid spacing. After discretization, equation (1) is written in residual form at each finite difference grid point. If the pressure and film thickness distribution represent a solution, the residual is zero. A residual expression representing the integral of the pressure over the solution region minus the specified load is appended to the system of residual equations. The central film thickness is used as a variable to control the integral of the pressure (load capacity). In obtaining a solution, an initial pressure distribution and central film thickness are assumed. An iterative scheme, based on the Newton-Raphson procedure

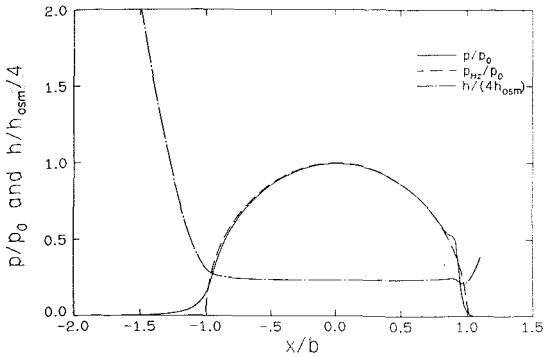

Fig. 3(a) Pressure distribution and film thickness

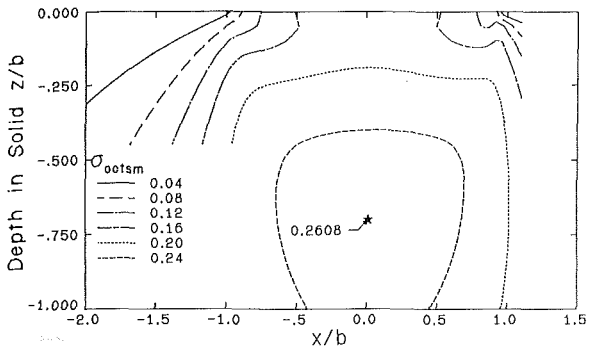

Fig. 3(b) Subsurface octahedral shear stress contours

Fig. 3 Reference smooth surface solution

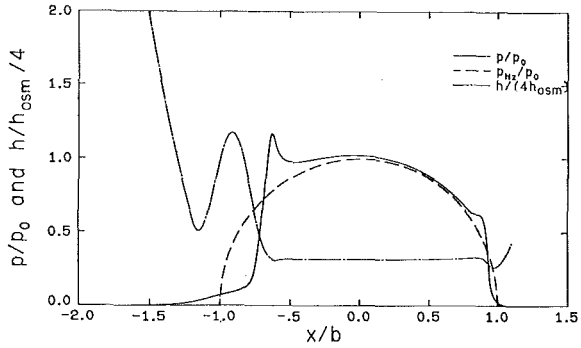

Fig. 4(a) Pressure distribution and film thickness

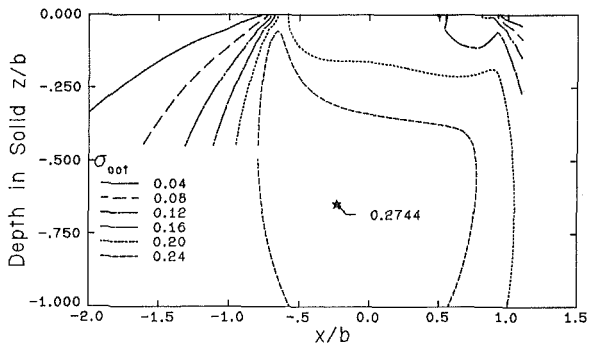

Fig. 4(b) Subsurface octahedral shear stress contours

Fig. 4 Effect of furrow located in the inlet, $\Delta = -5.34$, $x^*/b = -0.9$

for a system of equations, is used to drive the residuals to zero.

Data on the subsurface shear stresses are obtained by calculating the octahedral shear stress which, in terms of principal stresses, is given by:

$$\tau_{oct} = \frac{1}{3}\left[(\sigma_1 - \sigma_2)^2 + (\sigma_2 - \sigma_3)^2 + (\sigma_3 - \sigma_1)^2\right]^{1/2}. \quad (8)$$

The stress calculation is based on the work of Dowson, Higginson, and Whitaker [22].

Results

Solutions to the line contact EHD lubrication problem are presented in this section for the surface irregularities described previously. These solutions were obtained in order to investigate the effects of location (within and around the Hertzian region) and geometry of the irregularities on film thickness, pressure distribution and subsurface octahedral shear stresses.

The results to be presented are given in terms of the following nondimensional parameters: $\bar{W}$, $\bar{U}$, $\bar{G}_1$, $\bar{G}_2$, $\bar{P}_1$, $\bar{A}$, and $\bar{B}$.

This set of nondimensional parameters is sufficient to fully specify the solution of the smooth surface EHD line contact problem. The groupings for load, speed, material, and density parameters are those used by Dowson and Higginson [21]. The nondimensional parameters used for computational purposes were different from the parameters listed above and were chosen to insure a computational technique that would result in a minimum of round-off error.

The geometry of the irregularities is described in terms of dimensionless height and width parameters given by:

$$d_i/h_{osm} \text{ and } l_j/b;\ i = 1,2,3;\ j = 1,2,3,4$$

For all the surface irregularities considered in this paper, the parameter d_2/h_{osm} is given the symbol Δ while the parameter $l_2/b = l_3/b$ is given the symbol C. All the results to be presented have the following common nondimensional parameters: $\bar{W} = 0.75 \times 10^{-4}$, $\bar{U} = 0.31 \times 10^{-11}$, $\bar{G}_1 = 5000$, $\bar{G}_2 = 600$, $\bar{A} = 132$, $\bar{B} = 383$, and $C = 0.3$. Various values of $\bar{G}_1$, $\bar{G}_2$, $\bar{A}$, and $\bar{B}$ have been used or suggested in the past for steel lubricated with mineral oils [11, 20, 21]. The values used in this paper are representative of those used in these earlier investigations. Because of limited space, only some representative results are given. Additional results can be found in [18].

For the data presented in Figs. 3 through 7, in addition to the parameters given above, a value of $\bar{P}_1 = 0.76 \times 10^{-3}$ is used. This value of $\bar{P}_1$ is somewhat lower than that used in [11]. However, because of the higher initial slope for the pressure-viscosity model used in this paper relative to the pressure-viscosity model used in [11], the lubricant viscosity at the break points is approximately the same for the two models. In Figs. 3 through 7, the figures labeled "*a*" show the EHD pressure distribution and the dry contact Hertzian pressure distribution both normalized by the Hertzian peak pressure. In addition, these figures show the film thickness which is normalized by the central film thickness (h_{osm}) obtained from the EHD lubrication of two smooth surfaces in pure sliding. This film thickness is further scaled by a factor of four to more appropriately position the profile in the figures. The figures labeled "*b*" in Figs. 3 through 7 show a map of the lines of constant values of octahedral shear stress in the subsurface region directly beneath the contact area. These stresses are normalized on the peak Hertzian pressure.

Figure 3 shows the film thickness profile, pressure distribution, and octahedral shear stress field for two smooth surfaces in pure sliding. These plots are used as a reference in discussing the results to be presented for the simple furrow. The stress contours follow those predicted by Poritsky [23] for the Hertzian contact, deviating slightly at the outlet region where the contours are drawn closer to the surface near the outlet pressure rise. The maximum value of the subsurface octahedral shear stress is 0.2608 p_0 and it occurs on the line $x = 0$ at the depth of $z/b = -0.70$.

In Figs. 4 through 7, a furrow having $\Delta = -5.34$ is shown at

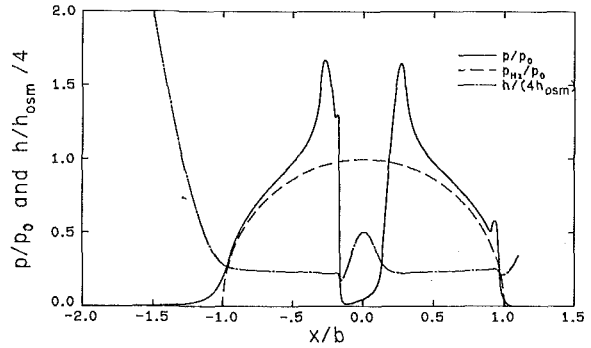

Fig. 5(*a*) Pressure distribution and film thickness

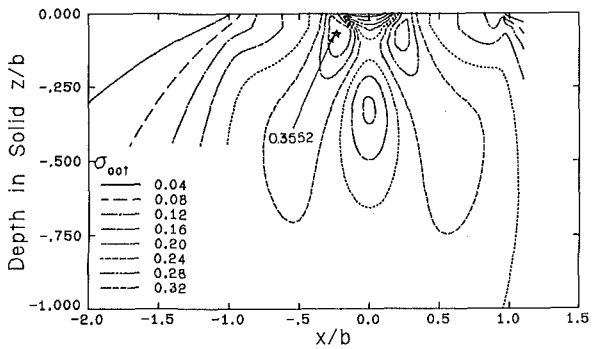

Fig. 5(*b*) Subsurface octahedral shear stress contours

Fig. 5 Effect of a centrally located furrow, $\Delta = -5.34$, $x^*/b = 0.0$

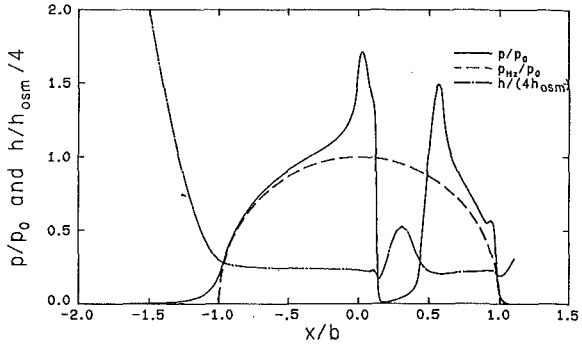

Fig. 6(*a*) Pressure distribution and film thickness

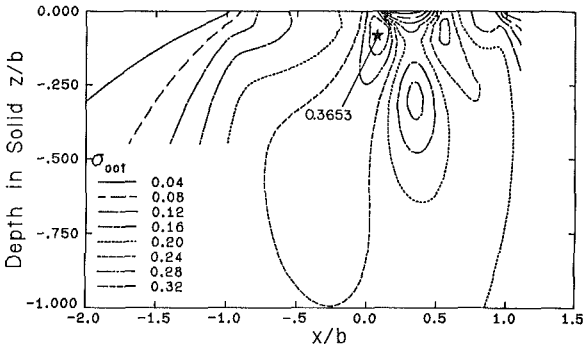

Fig. 6(*b*) Subsurface octahedral shear stress contours

Fig. 6 Effect of a furrow located in the outlet, $\Delta = -5.34$, $x^*/b = 0.3$

various locations in and around the Hertzian contact zone. The furrow center location is specified by the nondimensional parameter x^*/b. For $1.2 < x^*/b$ and $x^*/b < -1.7$, the solutions are the same as if no furrow were present.

Figure 4(*a*) shows the film thickness and pressure distribution for the furrow positioned at $x^*/b = -0.9$. For this location, the central film thickness increases 31 percent when compared with the reference case (Fig. 3(*a*)). As expected, the pressure distribution is modified by the presence of the furrow. The shallow pressure of the inlet sweep now extends to within the Hertzian region and there is a steep pressure rise on the outlet edge (right side) of the furrow. The remaining portion of the Hertzian zone remains similar to that of the reference case. When compared to the reference case, the corresponding stress contours shown in Fig. 4(*b*) are closer to the surface in the area around the outlet side (right side) of the furrow. The maximum value of octahedral shear stress has increased only slightly from the reference case and is located at about the same depth but about one-quarter of a Hertzian halfwidth toward the inlet side when compared to its location for the reference case.

With the same size furrow centrally located, the change in the central film thickness is small as shown in Fig. 5(*a*). The central film thickness in this case was taken to be the average of the film thicknesses at $x^*/b = \pm 0.5$. The notable point about the film thickness profile is the constriction at the leading edge of the furrow and the compression of the furrow depth to about one fourth its initial depth (from an undeformed depth of 5.34 h_{osm} to about 1.15 h_{osm}. The pressure distribution changes dramatically when compared with the reference case. The contact is essentially divided into two separate but coupled EHD solutions.

The stress contours shown in Fig. 5(*b*) have a distinctly different pattern than the reference case. There are two local maxima of stress values located at the inlet and outlet edges of the furrow. The largest value of octahedral shear stress is located at the inlet edge and is about 36 percent higher than the value of the octahedral shear stress in the reference case. The location of the maximum value of the octahedral shear stress has changed considerably, now it is located at a depth of about $z/b = -0.06$ and shifted laterally to the left to a position below the inlet edge of the furrow. The octahedral shear stress moves closer to the surface because of the high pressure peaks and pressure gradients occurring over a smaller contact area relative to the reference case.

Placing the furrow center at $x^*/b = 0.3$ results in the solution shown in Fig. 6. This case shows many of the same attributes of the case presented in Fig. 5. The film thickness constricts at the inlet side of the furrow as well as the overall outlet. The central film thickness is essentially the same as the reference case, varying by only 4 percent. The octahedral shear stress contours, shown in Fig. 6(*b*), show two local maxima as in the previous case. The maximum value octahedral shear stress occurs at a depth of $z/b = -0.07$ and is below the inlet edge of the furrow. The value of the maximum stress is about 40 percent larger than the reference case.

Figure 7 shows the solution for the furrow center located at $x^*/b = 0.8$. The pressure rises to a peak on the inlet side of the furrow in a similar manner to the previous two cases presented. The pressure drops to near zero within the furrow, begins to rise again at the outlet side of the furrow and drops back to zero just outside the dry contact Hertzian zone.

The film profile resembles the reference case throughout much of the contact up to the inlet side of the furrow. The central film thickness is about 4 percent less than that of the reference case. Also there is a constriction on the inlet edge of the furrow but the outlet edge of the furrow prevents the forming of the usual constriction at the exit.

The octahedral shear stress contours, shown in Fig. 7(*b*), again have local maxima below the inlet and outlet edges of the furrow. The overall maximum octahedral shear stress is below the inlet edge of the furrow at the depth of $z/b = -0.06$ and is 25 percent larger than the maximum found in the reference case.

The furrow with a non-dimensional depth of $\Delta = -5.34$ is chosen to illustrate the change in location of the maximum octahedral shear stress as the furrow center takes on various

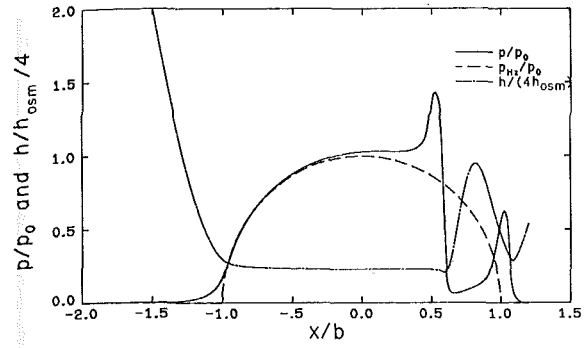

Fig. 7(*a*) Pressure distribution and film thickness

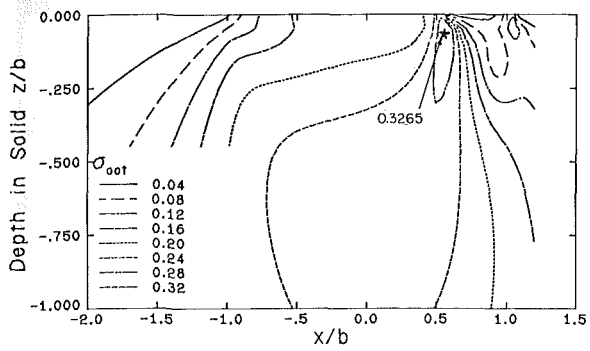

Fig. 7(*b*) Subsurface octahedral shear stress contours

Fig. 7 Effect of furrow located in the outlet, $\Delta = -5.34$, $x^*/b = 0.8$

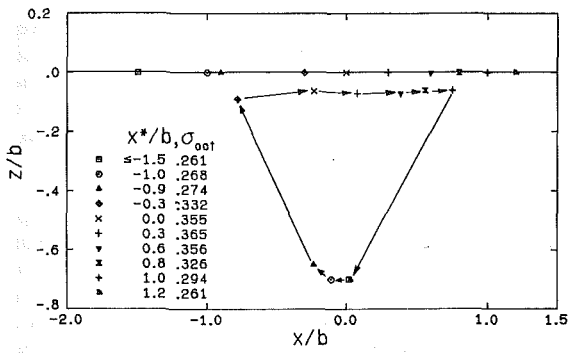

Fig. 8 Maximum octahedral shear stress locations as a function of furrow locations, $\Delta = -5.34$ (symbols below the line $z/b = 0$ indicate stress locations. Corresponding symbols on the line indicate furrow center locations. The legend indicates the level of stress of each symbol).

positions in the contact. Figure 8 shows the octahedral shear stress maxima for various values of x^*/b. Each symbol in the subsurface region indicates the location of the maximum stress while the corresponding symbol on the line $z/b = 0$ indicates the location of the center of the furrow. The arrows connecting the symbols indicate the movement of the maximum stress as the furrow is moved from inlet to outlet. With the furrow outside the inlet region ($x^*/b \leq -1.5$), the maximum value of the octahedral shear stress occurs at the same location as for the reference case. This location moves slightly to the left and then toward the surface for $x^*/b = -1.0$ and -0.9, respectively. For $-0.3 \leq x^*/b \leq 1.0$, the maximum value of the octahedral shear stress occurs at the depth of less than $z/b = -0.10$ and is located below the inlet edge of the furrow where the pressure peaks occur. With the furrow located at $x^*/b \geq 1.2$, the position of the maximum octahedral shear stress returns to the same location as the reference case. The maximum value of octahedral shear stress is located closest to the surface ($z/b = -0.06$) when the groove center is at $x^*/b = 0.0$ and 0.8.

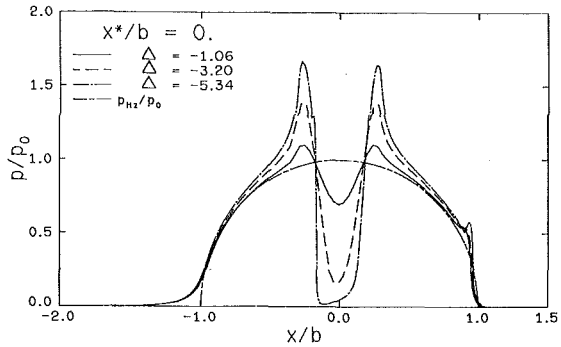

Fig. 9(*a*) Pressure distribution

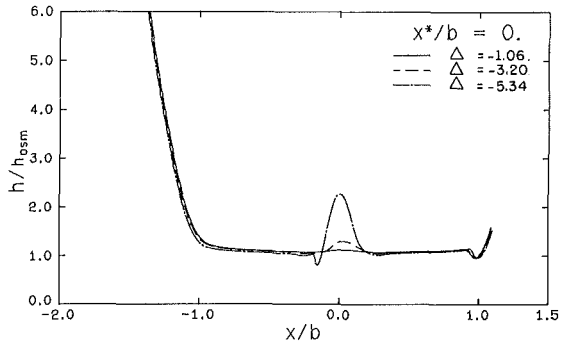

Fig. 9(*b*) Film thickness

Fig. 9 Effect of furrow depth on EHD lubrication for three values of Δ

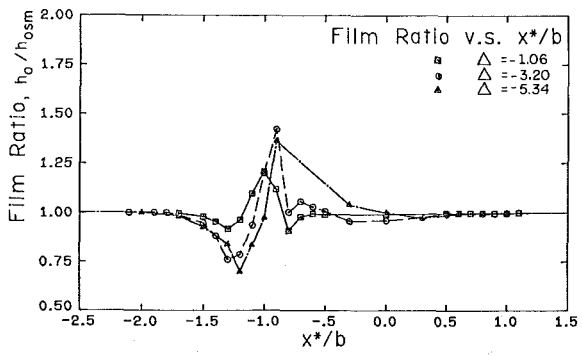

Fig. 10 Central film thickness ratio as a function of furrow position for three furrow depths

The influence of the depth of centrally located furrows on the film thickness and pressure distribution is shown in Fig. 9. As expected, Fig. 9(*a*) shows that, as Δ increases, the pressure peaks on both sides of the furrow become higher and the pressure at the furrow center approaches zero. The film thickness shown in Fig. 9(*b*) is essentially the same outside the furrow area for all three furrow depths considered.

To illustrate how film thickness is influenced by the presence of a furrow, a graph synthesizing the results for the central film thickness obtained from 65 solutions is shown in Fig. 10. The data for this graph are for three non-dimensional furrow depths of $\Delta = -1.06$, -3.20, and -5.34. The region of influence for the furrow is within the range $-2.0 < x^*/b < 0.5$. The general trend for all furrows considered is the same. For furrow locations approaching the inlet side of the Hertzian region, there is a central film thickness reduction below that of the reference case. Within a narrow range near the inlet edge of the Hertzian zone, there is a film thickness increase above that of the reference case. In all cases the film thickness ratio approaches 1.0 as the center is located toward the exit side of the Hertzian contact.

The same phenomenon of film reduction, increase and subsequent approach to a lower value was observed by Cusano and Wedeven [17] as a surface irregularity was moved

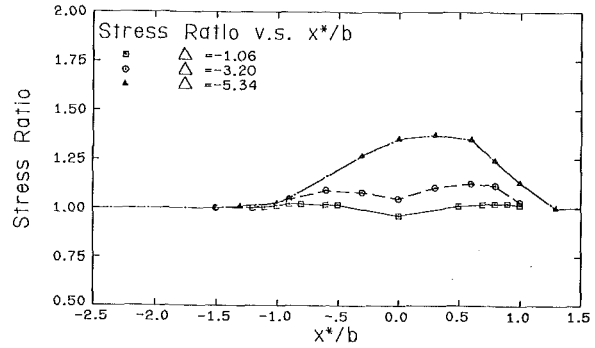

Fig. 11 Maximum subsurface octahedral shear stress ratio ($\sigma_{oct}/\sigma_{octsm}$) as a function of furrow position

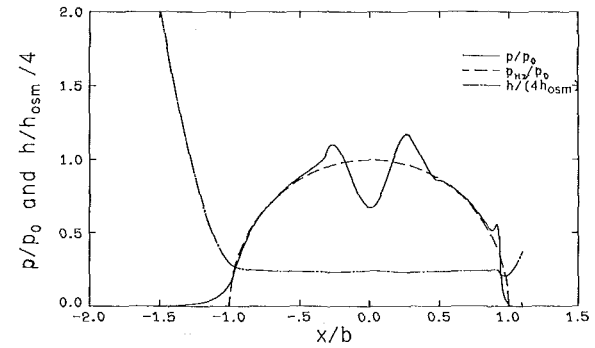

Fig. 12 Effect of furrow with an outlet side build-up edge on pressure distribution and film thickness, $x^*/b = 0.0$, $\Delta = -1.06$

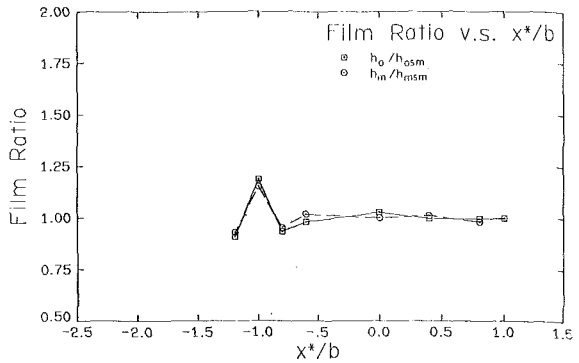

Fig. 13 Central and minimum film thickness ratios for a furrow with an outlet side built-up edge, $\Delta = -1.06$

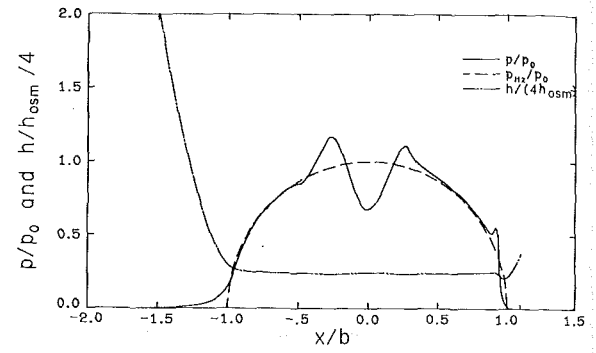

Fig. 14 Effect of furrow with an inlet side built-up edge on pressure distribution and film thickness, $x^*/b = 0.0$, $\Delta = -1.06$

through the inlet and central region of an EHD point contact. Since their data were obtained for a ball with a dent in contact with a plate, the present results and those in [17] are not directly comparable. However, the flow in the center of an EHD point contact is mainly velocity-induced and a single dent of diameter small enough compared to the Hertzian circle would not allow significant side leakage. The film thickness in a band upstream and downstream of the dent would be expected to behave much like that of a furrow in line contacts.

The effects of furrow location and depth on the maximum value of octahedral shear stress are shown in Fig. 11. The stress ratio is defined as the ratio of the maximum value of the octahedral shear stress of the case indicated to that of the reference case. Figure 11 shows this stress ratio as a function of furrow center location for each furrow depth presented. The stress is not significantly influenced by the furrow with the smallest depth ($\Delta = -1.06$). The magnitude changes by less than 4 percent and the location of the maximum octahedral shear stress remains at about the same location as that of the reference case. There is a more significant change in stress when the dimensionless furrow depth is increased to $\Delta = -3.20$. The maximum value of octahedral shear stress increased 12.5 percent above the reference value when this furrow is located at $x^*/b = 0.8$. As expected, the largest increase in the maximum value of the octahedral shear stress occurs with the deepest furrow considered ($\Delta = -5.34$). The stress ratio curve for this furrow depth peaks when the furrow is located at $x^*/b = 0.3$. At this location the maximum value of the octahedral shear stress is 40 percent greater than the smooth surface reference. Note that for all cases considered, the only significant increase in the stress ratio occurs when the center of furrows is located within the Hertzian zone.

If a furrow is produced in a metal surface due to debris, machining or assembly damage, the metal flow will frequently cause a small protrusion at one or both edges of the furrow. In [17], these protrusions or built-up edges were found to cause large local film thickness variations in the areas where they were located which also implied very large pressure variations in these areas. In addition to furrows with built-up edges, another surface irregularity which has practical significance is the asperity. Limited data will be given on the effects of furrows with built-up edges and asperities on both film thickness and pressure distribution in line contacts.

In obtaining the following data, the breakpoint, $\bar{P}_1$, was increased from 0.76×10^{-3} to 0.91×10^{-3}. This change will bring the breakpoint to a value closer to that suggested in [20] and used in [11]. It should be noted that as long as $\bar{P}_1$ represents a pressure which is larger than the pressure in the inlet region of the Hertzian contact, moderate changes in $\bar{P}_1$ will not appreciably change the results presented in this paper.

In Fig. 12 the pressure distribution and film profile are shown for the furrows with an outlet (right side) built-up edge. The furrow is located at $x^*/b = 0.0$. Using the notation of Fig. 1, the geometric parameters used to obtain these data are: $l_1/b = 0.0$, $l_4/b = 0.20$, $d_1/h_{osm} = 0.0$, $\Delta = d_2/h_{osm} = -1.06$ and $d_3/h_{osm} = 0.21$. The pressure distribution shown in Fig. 12 is similar to that shown in Fig. 11 for the same value of Δ except that, because of the built-up edge, the pressure peak on the outlet side of the furrow is both wider and higher compared with the pressure peak on the inlet side. The film shape has been deformed in such a way as to essentially eliminate both the furrow and built-up edge, leaving an almost constant film thickness in the central region. The pressure distribution and film profile remain essentially the same as the smooth surface case both upstream and downstream of the defect.

Figure 13 shows the changes in both central and minimum film thicknesses as the defect is positioned at various locations in the Hertzian contact region. The only significant changes in central and minimum film thicknesses occur with the defect positioned in the inlet region.

Film thickness and pressure distributions for a centrally located furrow with an inlet built-up edge are shown in Fig. 14. The nondimensional geometric parameters for this defect are: $l_1/b = 0.20$, $l_4/b = 0.0$, $d_1/h_{osm} = 0.21$, $\Delta = d_2/h_{osm} =$

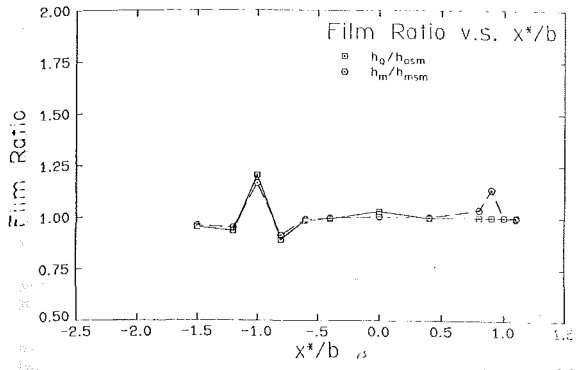

Fig. 15 Central and minimum film thickness ratios for a furrow with an inlet side built-up edge, $\Delta = -1.06$

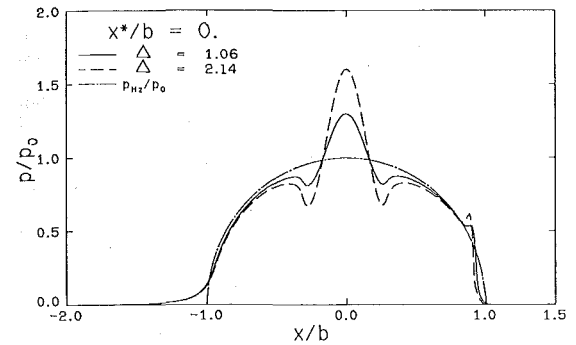

Fig. 16(*a*) Pressure distribution

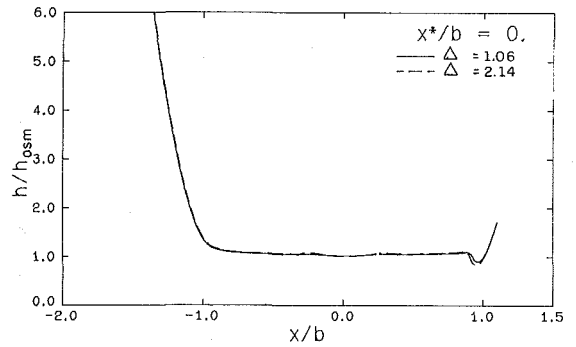

Fig. 16(*b*) Film thickness

Fig. 16 Effect of asperity height on EHD lubrication for a centrally located asperity

-1.06 and $d_3/h_{osm} = 0.0$. As expected, the shapes and amplitudes of the pressure peaks on each side of the furrow are opposite to those shown in Fig. 12. Again the film thickness distribution is approximately the same as the smooth surface case. The film thickness as a function of the position of the furrow is shown in Fig. 15. The changes seen are similar to that shown in Fig. 13. A notable point in this case is that the presence of the furrow in the vicinity of the usual location of the outlet constriction has increased the minimum film thickness above the smooth surface values by about 14 percent.

Built-up edges were observed to cause large film thickness variations from the smooth surface value in [17]. The reason for not observing such large variations in this study is because the height of the built-up edges and depths of the grooves (normalized on the smooth surface central film thickness) are smaller than the heights and depths considered in [17].

The pressure distributions and film thickness profiles for two centrally located asperities are shown in Fig. 16. Note that, geometrically, these asperities are described by the same parameters as a simple furrow except Δ is positive instead of being negative. From Fig. 16(*a*) it is seen that the decrease in pressure at the edges of the asperities is larger for the larger asperity. This decrease is caused by the relatively large surface deformation at the edges of the asperities. The film thickness profiles, shown in Fig. 16(*b*), are nearly the same throughout the inlet and central regions. For $\Delta = 1.06$ and 2.14, the central film thickness values are, respectively, 2.2 percent and 3.3 percent smaller than the smooth surface case, while the minimum film thickness values are, respectively, 4.2 percent and 18 percent smaller than the smooth surface case.

For $\Delta = 1.06$, both central and minimum film thicknesses do not vary substantially from the smooth surface value as the asperity is located at various positions in the Hertzian region. The central film thickness is never more than 2.5 percent greater than the smooth surface case and up to 14 percent smaller. The minimum film thickness is never more than 1 percent greater than the smooth surface case and up to 14.5 percent smaller. The central film thickness is primarily influenced by the presence of the asperity in the inlet region at $x^*/b \approx -1.0$. The minimum film thickness is influenced by the asperity located near the inlet, in the same manner as the central film thickness, and at the outlet where there is an interaction between the asperity and the outlet constriction.

The maximum value of the octahedral shear stress for the asperity follows the same trends as the simple furrow as the asperity height is increased relative to the central film thickness. For an asperity with $\Delta = 2.14$, the maximum value of the octahedral shear stress is 25 percent larger than the smooth surface case and it is located at $z/b = -0.15$ compared to $z/b = -0.70$ for the smooth surface case.

Discussion

The results presented in this paper show the effects of single surface irregularities on the film thickness profile, pressure distribution and octahedral shear stress in sliding line contacts under isothermal conditions. Similar results have been obtained by Cheng and Bali [11] for defects located in the inlet region. The values of $\bar{G}_1$, and $\bar{U}$ in this study differ from those used by Cheng and Bali and, therefore, prevent a meaningful direct comparison of results. The kinematic conditions analyzed in this study as well as those in [11] should result in an upper bound on both film thickness and pressure variations. This upper bound has been implied by the experimental results given in [13, 17]. Therefore, any other kinematic conditions such as pure sliding in which the defects are moving, combined rolling and sliding or pure rolling should have less influence on film thickness and pressure, for the same operating conditions and defect geometry, than the influence observed in this paper.

The results presented show that surface irregularities can significantly influence the lubrication process in lubricated concentrated contacts. These irregularities can cause high peak fluid pressures which influence the octahedral shear stresses in the metal. These stresses tend to increase locally in the region directly below a pressure peak and high pressure gradient caused by the irregularities. If the localized pressure is high enough, the location of the maximum value of the octahedral shear stress will move from approximately the location of the dry Hertzian maximum octahedral shear stress to a location much closer to the surface and directly below the localized pressure peak. A similar phenomenon is apparent in the data presented by Dowson, Higginson and Whitaker [22] for the maximum shear stress. The increase in and movement closer to the surface of the maximum value of the octahedral shear stress due to localized pressure peaks and large pressure gradients caused by surface irregularities can shorten the fatigue life of machine elements.

Surface irregularities can also influence scuffing failures in

machine elements. All the surface irregularities studied have caused position-dependent changes in the film thickness within the contact. In many cases, the central film thickness decreased significantly from the smooth surface values, some as much as 32 percent (see Fig. 10). Such film thickness reductions can lead to increased scuffing failures.

The effects of surface irregularities on the EHD lubrication process can depend on a number of factors which have not been analyzed in this study. Some of these factors are different kinematic conditions of the contacting surfaces, geometry of irregularities which could produce much larger variations in film thickness and pressure (including cavitation), and a more realistic rheological model for the lubricant which, could show less drastic changes in pressure and pressure gradients in the neighborhood of the irregularities. However, the results presented in this paper are useful in estimating the influence of surface irregularities on the EHD lubrication process and the resulting subsurface stress distributions.

Summary

Some of the more important observations which can be made about the effects of surface irregularities on the lubrication process in line EHD contacts under pure sliding conditions are:

1. Surface irregularities can significantly alter both pressure and film thickness distribution from their smooth surface values. These changes alter the state of stress in the subsurface region mainly by increasing the value of the maximum octahedral shear stress and bringing the location of this maximum closer to the surface.
2. The position of the converging or diverging portion of an irregularity in the critical inlet region respectively causes an increase or decrease in the film thickness in the contact.
3. The minimum film thickness is affected both by the general increase or decrease caused by changes in the inlet geometry, as mentioned above, and by local geometry deviations from the smooth surface at outlet constriction.
4. Film thickness constrictions within the contact area are observed with furrows when the pressure within the furrows approaches zero.
5. Subsurface stress levels increase to the greatest extent when irregularities are located in the outlet half of the contact.

References

1 Tzeng, S. T., and Saibel, E., "Surface Roughness Effect on Slider Lubrication," *Trans. ASLE*, Vol. 10, 1967, pp. 334–340.

2 Christensen, H., "Stochastic Models for Hydrodynamic Lubrication of Rough Surfaces," *Proc. Instn. Mech. Engrs.*, Vol. 184, Part 1, No. 55, 1970, pp. 1013–1022.

3 Christensen, H., "A Theory of Mixed Lubrication," *Proc. Instn. Mech. Engrs.*, Vol. 186, Part 1, No. 41, 1972, pp. 421–430.

4 Patir, N., and Cheng, H. S., "An Average Model for Determining Effects of Three-Dimensional Roughness on Partial Hydrodynamic Lubrication," ASME JOURNAL OF LUBRICATION TECHNOLOGY, Vol. 100, No. 1, 1978, pp. 12–17.

5 Patir, N., and Cheng, H. S., "Application of Average Flow Model to Lubrication Between Rough Sliding Surfaces," ASME JOURNAL OF LUBRICATION TECHNOLOGY, Vol. 101, 1979, pp. 220–230.

6 Chow, L. S. H., and Cheng, H. S., "The Effects of Surface Roughness on the Average Film Thickness Between Lubricated Rollers," ASME JOURNAL OF LUBRICATION TECHNOLOGY, Vol. 98, No. 1, 1976, pp. 117–224.

7 Fowles, P. E., "The Applications of Elastohydrodynamic Lubrication Theory to Individual Asperity-Asperity Collisions," ASME JOURNAL OF LUBRICATION TECHNOLOGY, Vol. 91, No. 3, 1969, pp. 464–476.

8 Lee, K., and Cheng, H. S., "Effect of Surface Asperity on Elastohydrodynamic Lubrication," NASA Contractor Report No. CR-2195, 1973.

9 Chow, L. S. H., and Cheng, H. S., "Pressure Perturbations in EHD Contacts due to an Ellipsoidal Asperity," ASME JOURNAL OF LUBRICATION TECHNOLOGY, Vol. 98, No. 1, 1976, pp. 8–15.

10 Cheng, H. S., "On Some Aspects of Microelastohydrodynamic Lubrication," *Surface Roughness Effects in Lubrication*, Proc. Fourth Leeds-Lyon Symp. on Tribology, Paper No. III(ii), 1977, pp. 71–79.

11 Cheng, H. S., and Bali, M., "Stress Distributions around Furrows and Asperities in EHL Line Contacts," *Solid Contact and Lubrication*, H. S. Cheng, and L. Keer, editors, ASME, 1980, pp. 205–222.

12 Jackson, A., and Cameron, A., "An Interferometric Study of the EHL of Rough Surfaces," *Trans. ASLE*, Vol. 19, No. 1, 1976, pp. 50–60.

13 Kaneta, M., and Cameron, A., "Effects of Asperities in Elastohydrodynamic Lubrication," ASME JOURNAL OF LUBRICATION TECHNOLOGY, Vol. 102, No. 3, 1980, pp. 374–379.

14 Wedeven, L. D., "Influence of Debris Dent in EHD Lubrication," *Trans. ASLE*, Vol. 21, No. 1, 1978, pp. 41–52.

15 Wedeven, L. D., and Cusano, C., "Elastohydrodynamic Film Thickness Measurements of Artificially Produced Surface Dents and Grooves," *Trans. ASLE*, Vol. 22, No. 4, 1979, pp. 369–381.

16 Cusano, C., and Wedeven, L. D., "Elastohydrodynamic Film Thickness Measurements of Artificially Produced Non-smooth Surfaces," *Trans. ASLE*, Vol. 24, No. 1, 1981, pp. 1–14.

17 Cusano, C., and Wedeven, L. D., "The Effect of Artificially Produced Defects on the Film Thickness Distribution in Sliding EHD Point Contacts," ASME JOURNAL OF LUBRICATION TECHNOLOGY, Vol. 104, No. 3, 1982, pp. 365–375.

18 Goglia, P. R., "The Effects of Surface Irregularities on the Elastohydrodynamic Lubrication of Sliding Line Contacts," Ph.D. Thesis, Dept. of Mech. and Ind. Engr., University of Illinois at Urbana-Champaign, 1982.

19 Timoshenko, S., and Goodier, J. N., *Theory of Elasticity*, Second Edition, McGraw-Hill, New York, 1951.

20 Allen, C. W., and Townsend, D. P., and Zaretsky, E. V., "Elastohydrodynamic Lubrication of a Spinning Ball in a Nonconforming Groove," ASME JOURNAL OF LUBRICATION TECHNOLOGY, Vol. 92, No. 1, 1970, pp. 89–96.

21 Dowson, D., and Higginson, G. R., *Elastohydrodynamic Lubrication*, Pergamon Press, New York, 1966.

22 Dowson, D., Higginson, G. R., and Whitaker, A. V., "Stress Distribution in Lubricated Rolling Contacts," *Fatigue in Rolling Contact*, Instn. Mech. Engrs., Paper 6, 1962, pp. 66–77.

23 Poritsky, H., "Stresses and Deflections of Cylindrical Bodies on Contact with Application to Contact of Gears and of Locomotive Wheels," ASME JOURNAL OF APPLIED MECHANICS, Vol. 17, No. 2, 1950, pp. 191–201.